

Temperature and polarization dependence of low-energy magnetic fluctuations in nearly-optimal-doped $\text{NaFe}_{0.9785}\text{Co}_{0.0215}\text{As}$

Yu Song,^{1,*} Weiyi Wang,¹ Chenglin Zhang,¹ Yanhong Gu,^{2,3} Xingye Lu,⁴ Guotai Tan,⁴ Yixi Su,⁵ Frédéric Bourdarot,⁶ A. D. Christianson,⁷ Shiliang Li,^{2,3,8} and Pengcheng Dai^{1,4,†}

¹*Department of Physics and Astronomy, Rice University, Houston, Texas 77005, USA*

²*Beijing National Laboratory for Condensed Matter Physics,*

Institute of Physics, Chinese Academy of Sciences, Beijing 100190, China

³*School of Physical Sciences, University of Chinese Academy of Sciences, Beijing 100190, China*

⁴*Center for Advanced Quantum Studies and Department of Physics, Beijing Normal University, Beijing 100875, China*

⁵*Jülich Centre for Neutron Science, Forschungszentrum Jülich GmbH, Outstation at MLZ, D-85747 Garching, Germany*

⁶*Institut Laue Langevin, 71 Avenue des Martyrs, 38042 Grenoble, France*

⁷*Quantum Condensed Matter Division, Oak Ridge National Laboratory, Oak Ridge, Tennessee 37831, USA*

⁸*Collaborative Innovation Center of Quantum Matter, Beijing, China*

We use unpolarized and polarized neutron scattering to study the temperature and polarization dependence of low-energy magnetic fluctuations in nearly-optimal-doped $\text{NaFe}_{0.9785}\text{Co}_{0.0215}\text{As}$, with coexisting superconductivity ($T_c \approx 19$ K) and weak antiferromagnetic order ($T_N \approx 30$ K, ordered moment $\approx 0.02 \mu_B/\text{Fe}$). A single spin resonance mode with intensity tracking the superconducting order parameter is observed, although energy of the mode only softens slightly on approaching T_c . Polarized neutron scattering reveals that the single resonance is mostly isotropic in spin space, similar to overdoped $\text{NaFe}_{0.935}\text{Co}_{0.045}\text{As}$ but different from optimal electron-, hole-, and isovalent-doped BaFe_2As_2 compounds, all featuring an additional prominent anisotropic component. Spin anisotropy in $\text{NaFe}_{0.9785}\text{Co}_{0.0215}\text{As}$ is instead present at energies below the resonance, which becomes partially gapped below T_c , similar to the situation in optimal-doped $\text{YBa}_2\text{Cu}_3\text{O}_{6.9}$. Our results indicate that anisotropic spin fluctuations in $\text{NaFe}_{1-x}\text{Co}_x\text{As}$ appear in the form of a resonance in the underdoped regime, become partially gapped below T_c near optimal doping and disappear in overdoped compounds.

PACS numbers: 74.25.Ha, 74.70.-b, 78.70.Nx

I. INTRODUCTION

A common theme of unconventional superconductivity in iron pnictides is the interplay between superconductivity and magnetism, with stripe-type antiferromagnetic (AF) fluctuations potentially playing the role of a bosonic glue that binds Cooper pairs¹⁻³. An experimental determination of the evolution of spin fluctuations across the superconducting dome in iron pnictides is therefore important for the understanding of these fascinating materials.

Parent compounds of iron pnictides such as $A\text{Fe}_2\text{As}_2$ ($A = \text{Ca}, \text{Sr}, \text{Ba}$) and NaFeAs are antiferromagnetically ordered and the corresponding spin waves with bandwidths ~ 0.1 eV have been carefully studied, and interpreted using effective Heisenberg models⁴⁻⁶ or itinerant electron models^{7,8}. Upon doping, magnetic order is gradually suppressed, and superconductivity is induced. Despite these changes, high-energy magnetic excitations resembling those in the parent compounds persist⁹⁻¹¹. On the other hand, low-energy magnetic excitations in the normal state are significantly modified, with profile of the excitations in the ab -plane becoming more elongated along the transverse and longitudinal directions upon electron- and hole-doping, respectively^{12,13}. Spin anisotropy gaps in the parent compounds are quickly

suppressed¹⁴, replaced by overdamped and diffusive spin excitations¹⁵. For superconducting samples, the most prominent change is the development of a spin resonance mode in the superconducting state, with intensity tracking the superconducting order parameter and also observed in other families of unconventional superconductors that exhibit strong magnetic fluctuations¹. The resonance mode appears as a significant enhancement of magnetic fluctuations in the superconducting state relative to the normal state, present only at well-defined momentum and energy transfers. Appearance of the resonance is usually accompanied by a complete or partial gapping of magnetic spectral weight below the resonance mode, with the total magnetic spectral weight being conserved.

Energy of the resonance mode (E_r) well inside the superconducting state has been proposed to universally scale with either the superconducting transition temperature T_c ($E_r \approx 4-6 k_B T_c$)^{16,17} or the superconducting gap 2Δ ($E_r \approx 0.64 \times 2\Delta$)¹⁸, although some iron-based superconductors deviate from such scalings¹⁹⁻²². The energy of the resonance mode was also found to track the superconducting order parameter as a function of temperature in optimal-electron-doped $\text{BaFe}_{1.85}\text{Co}_{0.15}\text{As}_2$ ²³. However, energies of the resonance modes in $\text{YBa}_2\text{Cu}_3\text{O}_7$ ²⁴, CeCoIn_5 ²⁵, $\text{FeTe}_{0.6}\text{Se}_{0.4}$ ²⁶, optimal-hole-doped $\text{Ba}_{0.67}\text{K}_{0.33}\text{Fe}_2\text{As}_2$ ¹¹

and electron-overdoped $\text{NaFe}_{0.935}\text{Co}_{0.045}\text{As}^{27}$ were found to only slightly soften on approaching T_c .

Recent angle-resolved photoemission spectroscopy (ARPES) measurements indicated spin-orbit coupling to be important for understanding the low-energy electronic structure of iron-based superconductors^{28–30}. Spin-orbit coupling also accounts for the “XYZ” spin anisotropy in parent compounds of iron pnictides^{31–33} and spin anisotropy in iron-based superconductors^{34,35}. Spin anisotropy is manifested in the resonance mode of superconducting iron pnictides up to optimal or slightly overdoped regime in electron- and hole-doped BaFe_2As_2 ^{36–38}, leading to resonance modes that exhibit an anisotropic part in addition to an isotropic part in spin space. The resonance mode becomes fully isotropic well into the overdoped regime³⁹. With unpolarized neutron scattering the two parts are difficult to resolve, and it has been suggested the two parts may have different origins⁴⁰.

In underdoped $\text{NaFe}_{1-x}\text{Co}_x\text{As}$ ($x = 0.015$) superconductor, two resonance modes are resolved even with unpolarized neutron scattering⁴¹. Using polarized neutron scattering, it was further found the mode at lower energy is anisotropic in spin space while the one at higher energy is isotropic⁴². With increasing doping the low-energy mode gradually loses spectral weight, while the mode at higher energy is present across the superconducting dome²⁰, however it is unclear how doping affects spin fluctuations in terms of spin anisotropy.

In this work, we use unpolarized and polarized neutron scattering to study the temperature and polarization dependence of spin fluctuations in nearly-optimal-doped $\text{NaFe}_{0.9785}\text{Co}_{0.0215}\text{As}$ superconductor exhibiting weak AF order with an ordered moment $\approx 0.02\mu_B$ ⁴³. A single resonance mode is observed, in contrast to underdoped $\text{NaFe}_{0.985}\text{Co}_{0.015}\text{As}^{41}$. We find intensity of the resonance mode follows the superconducting order parameter, but energy of the mode E_r is almost temperature-independent, softening only slightly on approaching T_c . This is different from the behavior in optimal-doped $\text{BaFe}_{1.85}\text{Co}_{0.15}\text{As}_2$, but similar to other unconventional superconductors^{11,24–27}. Polarized neutron scattering reveals the resonance to be mostly isotropic, different from electron-, hole- and isovalent-doped BaFe_2As_2 superconductors near optimal doping^{27,36,44}, which also exhibit an additional anisotropic component. Significant spin anisotropy is instead present below the resonance mode, in the form of remnant spectral weight inside a partial spin gap induced by superconductivity, similar to optimal-doped $\text{YBa}_2\text{Cu}_3\text{O}_{6.9}$ ⁴⁵. Spin anisotropy at these energies persists up to $T \approx 35$ K, and measurements of resistivity change under uniaxial stress indicates Curie-Weiss behavior down to a similar temperature. This finding confirms the link between deviation from Curie-Weiss behavior in nematic susceptibility and development of low-energy spin anisotropy, previously found in BaFe_2As_2 -derived superconductors³⁴. Combined with previous results⁴², our work establishes a systematic understanding of how spin anisotropy evolves with doping

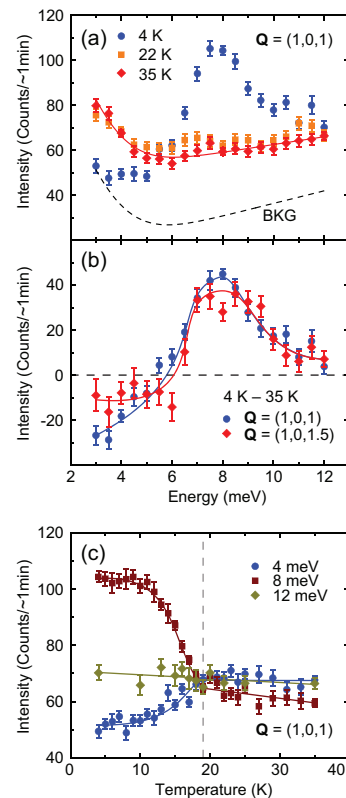


Figure 1: (Color online) (a) Constant- \mathbf{Q} scans at $\mathbf{Q} = (1, 0, 1)$ for $T = 4, 22$ and 35 K. The solid line is an empirical fit to data at 35 K. The dashed line is a fit to the background (BKG) intensity. (b) Comparison of difference between 4 K and 35 K for constant- \mathbf{Q} scans at $\mathbf{Q} = (1, 0, 1)$ and $(1, 0, 1.5)$. The solid lines are guides to the eye. (c) Temperature dependence of spin fluctuations for $E = 4, 8$ and 12 meV at $\mathbf{Q} = (1, 0, 1)$. The solid lines are guides to the eye. Data in this figure are obtained on HB-3 using unpolarized neutron scattering.

in superconducting $\text{NaFe}_{1-x}\text{Co}_x\text{As}$.

II. EXPERIMENTAL DETAILS

Single crystals of $\text{NaFe}_{0.9785}\text{Co}_{0.0215}\text{As}$ were grown using the self-flux method⁴⁶ and were previously studied using elastic neutron scattering⁴³ and time-of-flight neutron spectroscopy⁴⁷. Unpolarized inelastic neutron scattering measurements were carried out using the HB-3 thermal triple-axis spectrometer at the High Flux Isotope Reactor, Oak Ridge National Laboratory. Polarized inelastic neutron scattering measurements were carried out using the IN22 triple-axis spectrometer at Institut Laue-Langevin. Fixed $E_f = 14.7$ meV was used for both experiments. The experiment on HB-3 used a pyrolytic graphite monochromator, analyzer, and filter after the sample, the collimation used is $48'-40'$ -sample- $40'$ - $120'$. The experiment on IN22 used a Heusler monochromator and analyzer, and utilizes the CRYOPAD for longitudi-

nal polarization analysis. We adopt notation for the orthorhombic structural unit cell of NaFeAs ($a \approx b \approx 5.56$ Å, $c = 6.95$ Å), and aligned samples in the $[H, 0, L]$ scattering plane to access excitations at $\mathbf{Q} = (1, 0, L)$. For NaFe $_{1-x}$ Co $_x$ As displaying magnetic order, half-integer L -values correspond to AF zone centers and integer L -values correspond to AF zone boundaries along c -axis⁴⁸.

For polarized neutron scattering three neutron spin-flip (SF) cross sections σ_x^{SF} , σ_y^{SF} and σ_z^{SF} were measured, with the usual convention $x \parallel \mathbf{Q}$, $y \perp \mathbf{Q}$ in the scattering plane, and z perpendicular to the scattering plane. Magnetic scattering polarized along α -direction, M_α ($\alpha = y, z$), can be obtained from measured SF cross sections through $\sigma_x^{\text{SF}} - \sigma_y^{\text{SF}} \propto M_y$ and $\sigma_x^{\text{SF}} - \sigma_z^{\text{SF}} \propto M_z$ ³⁴. By comparison, unpolarized neutron scattering does not separate these two quantities, and the measured cross sections contain both M_y and M_z . With our experiment geometry, at $\mathbf{Q} = (1, 0, L)$, M_y is a combination of M_a and M_c whereas $M_z = M_b$. Spin-anisotropic magnetic fluctuations can be observed through differing σ_y^{SF} and σ_z^{SF} cross sections, and differing M_y and M_z .

III. RESULTS

A. Temperature Dependence of Spin Fluctuations From Unpolarized Neutron Scattering

Constant- \mathbf{Q} scans at $\mathbf{Q} = (1, 0, 1)$ for $T = 4$ K (well below T_c), 22 K (just above T_c) and 35 K (just above T_N) are compared in Fig. 1(a). Similar to slightly overdoped NaFe $_{0.935}$ Co $_{0.045}$ As, a single resonance mode forms at the expense of spectral weight at lower energies in the superconducting state²⁷. The results at 22 K and 35 K are similar, consistent with the small ordered moment of $\approx 0.02\mu_B$ ⁴³ having little impact on magnetic fluctuations below T_N . In Fig. 1(b), we compare the difference of magnetic intensity between 4 K and 35 K for $\mathbf{Q} = (1, 0, 1)$ and $\mathbf{Q} = (1, 0, 1.5)$. Whereas the resonance mode shows little dependence on L , reduction of spectral weight below the resonance mode is more significant for integer L . Given that in the normal state, magnetic fluctuations at AF zone center (half-integer L) is at least as strong as fluctuations at AF zone boundary along c -axis (integer L), the smaller reduction of spectral weight at AF zone center implies significant remnant spectral weight below the resonance mode at AF zone center in the superconducting state. Temperature dependence of the scattering at $\mathbf{Q} = (1, 0, 1)$ is shown for several representative energies in Fig. 1(c). At the resonance energy $E = 8$ meV, an order-parameter-like behavior is seen. Below the resonance, a clear reduction of spectral weight is observed. Above the resonance energy, intensity of magnetic excitations does not respond to the onset of superconductivity. Such temperature dependence is similar to other iron pnictide superconductors^{23,41}.

Constant- \mathbf{Q} scans at several temperatures below $T_c \approx 19$ K are shown in Fig. 2(a), subtracted by a fit to 35

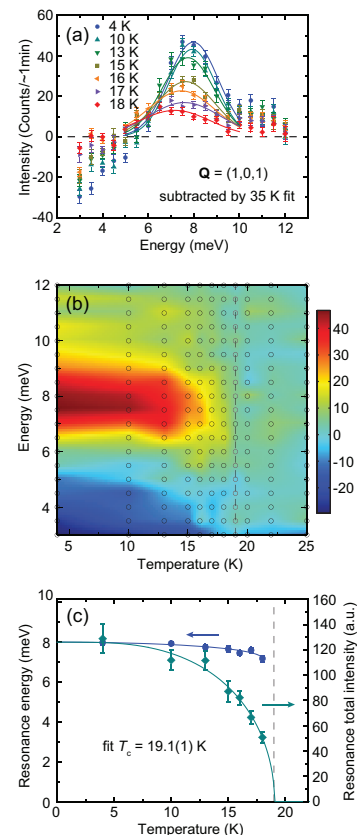


Figure 2: (Color online) (a) Constant- \mathbf{Q} scans at $\mathbf{Q} = (1, 0, 1)$ for several temperatures below T_c , subtracted by the empirical fit to 35 K data. The solid lines are fits to Gaussian peaks in the energy range $5 \leq E \leq 10$ meV. (b) Color-coded and interpolated temperature dependence of low-energy magnetic fluctuations. The empirical fit to 35 K data has been subtracted. The circles correspond to points where measurements were taken. (c) Temperature dependence for the center and the area of the resonance mode, obtained from Gaussian fits in (a). The solid line for the resonance energy is a guide to the eye, and the solid line for the total area is a fit to the superconducting order parameter⁴⁹. The dashed vertical lines represent $T_c \approx 19$ K. Data in this figure are obtained on HB-3 using unpolarized neutron scattering.

K data to highlight the resonance mode and reduction of spectral weight at lower energies. The data in Fig. 2(a) are color-coded and interpolated, as shown in Fig. 2(b) for a direct visualization. To quantitatively characterize temperature dependence of the resonance mode, data points in Fig. 2(a) with $5 \leq E \leq 10$ meV are fit to Gaussian peaks to extract energy and intensity of the mode, with results shown in Fig. 2(c). Whereas intensity of the resonance can be reasonably described by the BCS order parameter with $T_c \approx 19$ K⁴⁹, energy of the resonance only slightly softens from $E \approx 8$ meV to $E \approx 7$ meV.

An alternative way to extract temperature dependence for energy of the resonance mode is to directly examine the magnetic intensity in the superconducting state, without subtracting the normal state response, as shown

in Fig. 3. Results in Fig. 3(a) can be phenomenologically modeled as damped harmonic oscillator responses, with measured intensity $I(\mathbf{Q}, E) \propto \frac{\chi''(\mathbf{Q}, E)}{1 - \exp(-\frac{E}{k_B T})}$ and $\chi''(\mathbf{Q}, E) \propto \frac{E_0^2 \gamma E}{(E_0^2 - E^2)^2 + \gamma^2 E^2}$ ¹⁵. E_0 characterizes energy of the mode while γ characterizes damping of the mode. The resulting E_0 and γ for different temperatures are shown in Fig. 3(c) together with E_{\max} , the energy at which $\chi''(\mathbf{Q}, E)$ is maximized. As can be seen, both E_0 and E_{\max} change only slightly with temperature. While E_0 depends weakly on temperature, γ increases significantly with increasing temperature. Interestingly, the above analysis indicates appearance of the resonance mode in $\text{NaFe}_{0.9785}\text{Co}_{0.0215}\text{As}$ can be interpreted as removal of damping from an existing mode, a scenario recently proposed for $\text{Ce}_{1-x}\text{Yb}_x\text{CoIn}_5$ ⁵⁰. However, we note unlike $\text{Ce}_{1-x}\text{Yb}_x\text{CoIn}_5$, behaviors of the resonance mode in iron pnictides are also consistent with the spin-exciton scenario^{27,51}.

From analysis presented in Fig. 2 and Fig. 3, we demonstrate that energy of the resonance mode in $\text{NaFe}_{0.9785}\text{Co}_{0.0215}\text{As}$ depends weakly on temperature, this conclusion holds whether we analyze our data by subtracting the normal state response (Fig. 2) or not (Fig. 3).

B. Polarization of Spin Fluctuations From Polarized Neutron Scattering

Constant- \mathbf{Q} scans of the three SF cross sections σ_x^{SF} , σ_y^{SF} and σ_z^{SF} at $\mathbf{Q} = (1, 0, 0.5)$ were measured well below ($T = 2$ K) and just above T_c ($T = 21$ K), and are shown in Figs. 4(a) and (b). Magnetic fluctuations inside the superconducting state are clearly modified from their normal state counterpart, displaying both the resonance mode and a superconductivity-induced spin gap, in agreement with unpolarized neutron scattering results in Fig. 1. Despite such changes, spin anisotropy as indicated by differing σ_y^{SF} and σ_z^{SF} is observed below a similar energy ($E < 7$ meV) for both temperatures. The differences, $\sigma_x^{\text{SF}} - \sigma_y^{\text{SF}} \propto M_y$ and $\sigma_x^{\text{SF}} - \sigma_z^{\text{SF}} \propto M_z$, are shown in Figs. 4(c) and (d) for the two temperatures. In the superconducting state [Fig. 4(c)], while M_z is gapped for $E \lesssim 5$ meV, significant spectral weight in M_y remains. The remnant spectral weight in M_y therefore accounts for the partial gapping of spectral weight at half-integer L seen in unpolarized neutron scattering [Fig. 1(b)]. In the normal state [Fig. 4(d)], spin anisotropy is also observed, similar to electron- and hole-doped BaFe_2As_2 ^{36,37,52}, but different from isovalent-doped $\text{BaFe}_2\text{As}_{1.4}\text{P}_{0.6}$ ⁴⁴.

In BaFe_2As_2 -derived superconductors near optimal doping, a prominent anisotropic contribution to the resonance mode is also observed^{34,36,37,44}. Comparing the results in Figs. 4(c) and (d), while anisotropic fluctuations at $E = 6$ meV may be slightly enhanced in the superconducting state of nearly optimal-doped $\text{NaFe}_{0.9785}\text{Co}_{0.0215}\text{As}$, most of the anisotropic magnetic

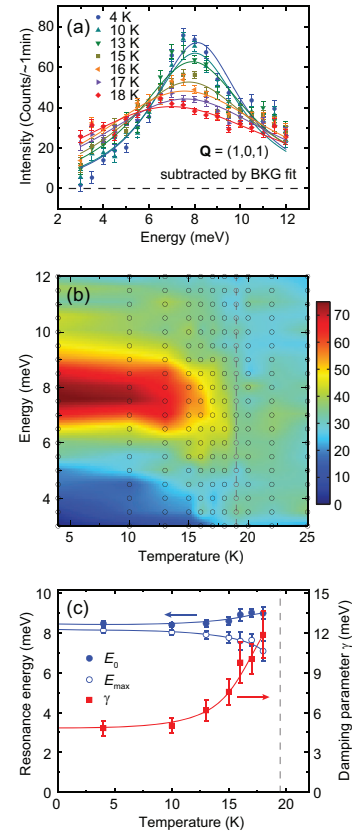


Figure 3: (Color online) (a) Constant- \mathbf{Q} scans at $\mathbf{Q} = (1, 0, 1)$ for several temperatures below T_c , subtracted by the fit to background (BKG) intensity. The solid lines are fits to damped harmonic oscillator responses in the energy range $3 \leq E \leq 12$ meV. (b) Color-coded and interpolated temperature dependence of low-energy magnetic fluctuations. The fit to background has been subtracted. The circles correspond to points where measurements were taken. (c) Temperature dependence for E_0 , E_{\max} and γ from damped harmonic oscillator fits in (a). The solid lines are guides to the eye. The dashed vertical lines represent $T_c \approx 19$ K. Data in this figure are obtained on HB-3 using unpolarized neutron scattering.

fluctuations reside below the resonance mode, becoming partially gapped inside the superconducting state. This conclusion is corroborated by temperature dependence of spin anisotropy measured for $E = 3$ and 5 meV, shown in Fig. 5. For $T \gtrsim 35$ K, both energies display $\sigma_y^{\text{SF}} \approx \sigma_z^{\text{SF}}$, indicating isotropic magnetic fluctuations [Figs. 5(a) and (b)]. The evolution of M_y and M_z as a function of temperature obtained from the differences $\sigma_x^{\text{SF}} - \sigma_y^{\text{SF}}$ and $\sigma_x^{\text{SF}} - \sigma_z^{\text{SF}}$ are shown in Figs. 5(c) and (d). For $E = 3$ meV, M_y increases on approaching T_c from above and is suppressed below T_c whereas M_z displays little temperature dependence above T_c and is also suppressed below T_c . For $E = 5$ meV, M_y displays little temperature dependence whereas M_z behaves similarly to $E = 3$ meV. At both energies, the magnetic fluctuations display clear spin anisotropy for $T \lesssim 35$ K but no enhancement is observed below T_c in either M_y or M_z . This coupled

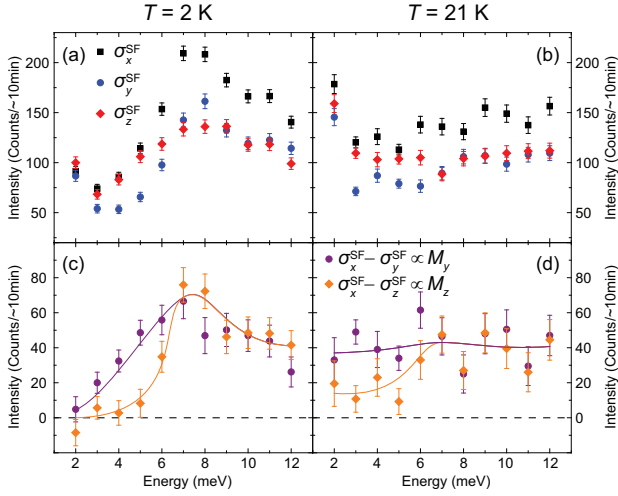


Figure 4: (Color online) Constant- \mathbf{Q} scans of σ_x^{SF} , σ_y^{SF} and σ_z^{SF} at $\mathbf{Q} = (1, 0, 0.5)$ (a) well below T_c ($T = 2$ K) and (b) just above T_c ($T = 21$ K). The differences $\sigma_x^{\text{SF}} - \sigma_y^{\text{SF}}$ and $\sigma_x^{\text{SF}} - \sigma_z^{\text{SF}}$, which are respectively proportional to M_y and M_z , are correspondingly shown in (c) and (d). The solid lines are guides to the eye. Data in this figure are obtained on IN22 using polarized neutron scattering.

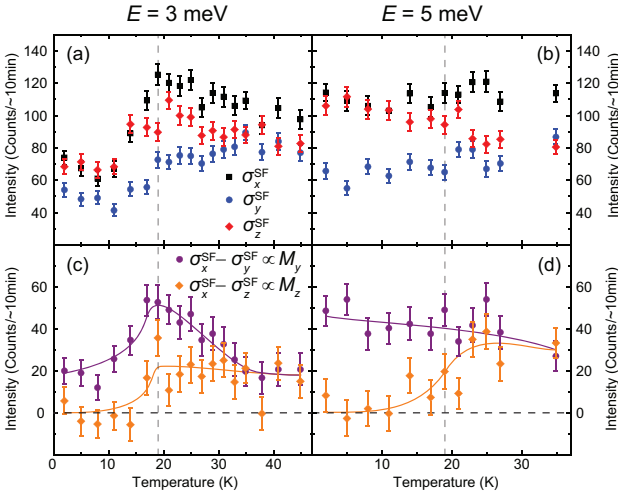


Figure 5: (Color online) Temperature dependence of σ_x^{SF} , σ_y^{SF} and σ_z^{SF} at $\mathbf{Q} = (1, 0, 0.5)$ for (a) $E = 3$ meV and (b) $E = 5$ meV. The differences $\sigma_x^{\text{SF}} - \sigma_y^{\text{SF}}$ and $\sigma_x^{\text{SF}} - \sigma_z^{\text{SF}}$, which are respectively proportional to M_y and M_z are correspondingly shown in (c) and (d). The solid lines are guides to the eye. The vertical dashed lines represent T_c . Data in this figure are obtained on IN22 using polarized neutron scattering.

with the observation that spin anisotropy is only present for $E < 7$ meV [Figs. 4(a) and (b)] suggests potential anisotropic fluctuations that become enhanced in the superconducting state could only exist for $5 < E < 7$ meV, although no such indication can be seen in the constant- \mathbf{Q} scans [Figs. 4(c) and (d)].

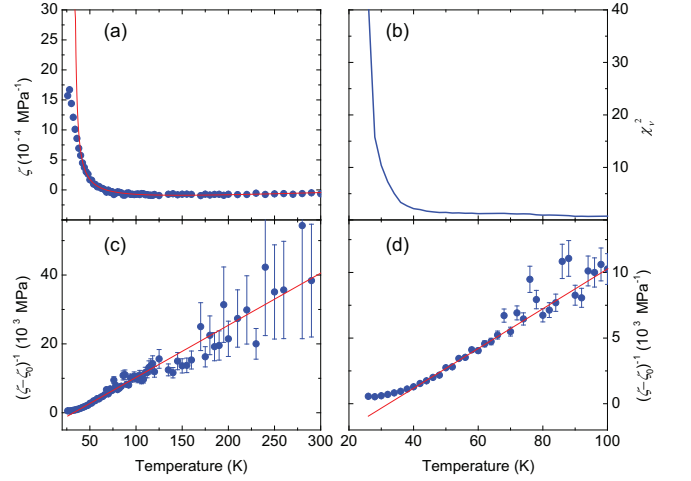


Figure 6: (Color online) (a) Resistivity change under uniaxial stress ζ along (100) direction for the orthorhombic unit cell [(110) direction for the tetragonal unit cell]. The solid red line is a CW fit for $T \geq 40$ K. (b) Reduced chi-squared from CW fits of data in (a), by setting the fitting ranges to be from different temperatures to 300 K. The same standard deviation is used for all measured data points to obtain reduced chi-squared, and is estimated from the standard deviation of data with $T > 100$ K. (c) $(\zeta - \zeta_0)^{-1}$ for the fit shown in (a), the error bars for ζ is estimated from standard deviation of data with $T > 100$ K, and the error bars for $(\zeta - \zeta_0)^{-1}$ is obtained through propagation of error. (d) Zoom-in of results in (c).

C. Resistivity Change Under Uniaxial Pressure

Previously, it was found the resistivity change under uniaxial strain (elastoresistance)⁵³ or stress^{54,55}, which acts as a proxy for the nematic susceptibility, displays Curie-Weiss (CW) temperature dependence in many iron-based superconductors. However, for electron- and hole-doped BaFe_2As_2 superconductors, deviations from CW behavior were found at temperatures above T_c , although CW behavior was found down to T_c in iso-valent-doped $\text{BaFe}_2\text{As}_{1.4}\text{P}_{0.6}$ ⁵³. It was noted that the temperatures at which nematic susceptibility deviate from CW behavior correspond to temperatures at which spin anisotropy onset in these systems, suggesting anisotropic magnetic fluctuations may be responsible for the deviation from CW behavior in nematic susceptibility³⁴.

Having established anisotropic magnetic excitations onset at $T \approx 35$ K in $\text{NaFe}_{0.9785}\text{Co}_{0.0215}\text{As}$ (Fig. 5), it would be interesting to check if CW behavior in nematic susceptibility holds down to a similar temperature. To this end, we measured resistivity change under uniaxial stress ζ using the device described previously⁵⁴, with stress applied along (100) direction of the orthorhombic unit cell [(110) direction of the tetragonal unit cell], and the result is shown in Fig. 6(a). The data is fit to the CW form $\zeta = \zeta_0 + \frac{A}{T - T_{\text{CW}}}$. To account for a weak upturn observed for $T \gtrsim 200$ K, ζ_0 is allowed to have a weak linear dependence on temperature, rather than being fully

temperature-independent.

A reasonable fit is obtained by fitting the data from 40 K to 300 K [solid red lines in Fig. 6(a)]. From the data and fit in Fig. 6(a), $(\zeta - \zeta_0)^{-1} = \frac{T - T_{CW}}{A}$ is shown in Figs. 6(c) and 6(d), with Fig. 6(d) zoomed in to focus on data with $T < 100$ K. Linear behavior in $(\zeta - \zeta_0)^{-1}$ is seen from 300 K down to $T \approx 40$ K [Fig. 6(d)], and clear deviation from linear behavior is seen at lower temperature. From the fit in Fig. 6(a) we obtain $T_{CW} \approx 31$ K and $A^{-1} \approx 135$ MPa/K. The value of T_{CW} in our sample is between T_{CW} of NaFeAs and NaFe_{0.986}Ni_{0.015}As, and the value of A^{-1} is reasonably close to those reported in NaFe_{1-x}Ni_xAs⁵⁵, after adjusting for a Fermi surface factor $\kappa \approx 11$ resulting in $A_n^{-1} \approx 12$ MPa/K⁵⁵. However, we found that both T_{CW} and A^{-1} depend on the fitting range we use. Fitting the data from 30 K to 300 K we obtain $T_{CW} \approx 21$ K and $A^{-1} \approx 60$ MPa/K, while fitting the data from 50 K to 300 K we obtain $T_{CW} \approx 38$ K and $A^{-1} \approx 234$ MPa/K.

Goodness of fit strongly depends on the chosen fitting range, as can be seen in reduced chi-squared (χ_ν^2) obtained by fitting starting from different temperatures to 300 K, as shown in Fig. 6(b). While χ_ν^2 changes only modestly when fitting starts from temperatures $T \gtrsim 40$ K, it increases dramatically when the fitting starts from lower temperatures. This indicates ζ deviates from CW behavior below $T \approx 40$ K, close to $T \approx 35$ K below which spin anisotropy develops. The persistence of CW behavior down to a similar temperature is also observed in nearly-optimal-doped NaFe_{0.985}Ni_{0.015}As⁵⁵. These results indicate compared to electron-doped BaFe₂As₂⁵³, CW behavior in nematic susceptibility persists to lower temperatures in electron-doped NaFeAs, and confirms the link between development of anisotropic magnetic fluctuations and the nematic susceptibility deviating from CW behavior³⁴.

IV. DISCUSSION AND CONCLUSION

Our polarized neutron scattering results reveal that anisotropic spin fluctuations in nearly-optimal-doped NaFe_{0.9785}Co_{0.0215}As become partially suppressed inside the superconducting state, lacking the prominent anisotropic resonance mode that is enhanced with the onset of superconductivity, seen in BaFe₂As₂-derived superconductors nearly optimal doping. Instead, the presence of anisotropic fluctuations that exist below an isotropic resonance mode is similar to what is observed in optimal-doped YBa₂Cu₃O_{6.9}⁴⁵. Previously, it was found that of the two resonance modes in underdoped NaFe_{0.985}Co_{0.015}As, the mode at lower energy is anisotropic while the one at higher energy is isotropic⁴². With Co-doping, the resonance mode at lower energy becomes suppressed near optimal doping, while the mode at higher energy persists across the superconducting dome²⁰. These findings are consistent with our present conclusion that no prominent anisotropic resonance mode is present in nearly-optimal-doped NaFe_{0.9785}Co_{0.0215}As.

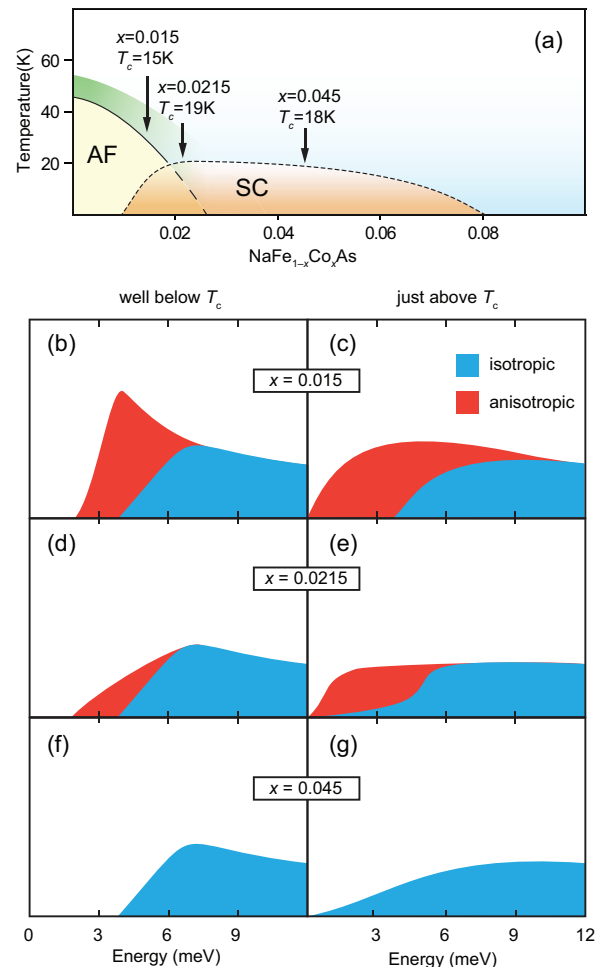


Figure 7: (Color online) (a) Schematic phase diagram of NaFe_{1-x}Co_xAs⁵⁹. The three concentrations for which polarized neutron scattering have been carried out are marked by arrows. Sketches of isotropic and anisotropic magnetic fluctuations well below T_c and just above T_c for $x = 0.015$ are respectively shown in (b) and (c). Similar sketches for $x = 0.0215$ are shown in (d) and (e), and for $x = 0.045$ in (f) and (g).

Combined with previous results⁴², our present work allows for a systematic understanding of how anisotropic spin dynamics evolve in NaFe_{1-x}Co_xAs, as sketched in Fig. 7. Three samples have been so far studied, representative of underdoped ($x = 0.015$), optimal-doped ($x = 0.0215$) and overdoped ($x = 0.045$) regions of the phase diagram [Fig. 7(a)]. As can be seen, with increasing doping, anisotropic fluctuations are gradually suppressed, evolving from a resonance mode in the underdoped regime [Fig. 7(b)] to remnant spectral inside a superconductivity-induced partial spin gap near optimal doping [Fig. 7(d)], and disappearing in the overdoped regime [Fig. 7(f)].

It is noteworthy that anisotropic fluctuations typically appear above T_c [Figs. 7(c) and (e)], and develop into an anisotropic resonance mode or become par-

tially gapped inside the superconducting state^{34–37,42,52}. BaFe₂As_{1.4}P_{0.6} appears to be an exception, with anisotropic spin fluctuations only present in the superconducting state⁴⁴.

Anisotropic fluctuations at the stripe-type AF ordering wave vector in iron pnictides and chalcogenides reported so far can be viewed to fall within situations of Fig. 7. In one extreme, there is FeSe with the resonance entirely anisotropic (although it is unclear at what energy fluctuations become isotropic), and in the other extreme the resonance is fully isotropic as found in overdoped iron pnictides^{39,42}. In most systems reported so far, it is observed $M_y \geq M_z$, namely c - or a -axis (in-plane longitudinal direction at the stripe vector) polarized excitations are at least as intense as b -axis (in-plane transverse direction at the stripe vector) polarized excitations. However, recently it was reported that in underdoped Ba(Fe_{0.955}Co_{0.045})₂As₂ with coexisting magnetic order and superconductivity, the resonance mode has no isotropic component⁵⁶, different from the behaviors depicted in Fig. 7. A possible reason is that the ordered moment in Ba(Fe_{0.955}Co_{0.045})₂As₂ is $\approx 0.2\mu_B/\text{Fe}$, much larger than $\approx 0.03\mu_B/\text{Fe}$ seen in underdoped NaFe_{0.985}Co_{0.015}As⁴³, and therefore features stronger interplay between magnetic order and the resonance mode.

While we have linked the development of spin anisotropy with deviation from CW behavior in nematic susceptibility in iron pnictides near optimal doping, diverging longitudinal fluctuations in BaFe₂As₂ just above T_N ⁵⁷ does not have the same effect on nematic susceptibility, with CW nematic susceptibility persisting down to T_N ⁵⁸. A possible cause for this difference is that whereas divergent longitudinal fluctuations in BaFe₂As₂ just above T_N have $M_a > M_b \approx M_c$ ⁵⁷, anisotropic fluctu-

ations in the normal state of BaFe₂As₂-derived superconductors near optimal doping exhibit $M_a \approx M_c > M_b$ ^{34,52}. The differing character of polarization may account for the different effects on the nematic susceptibility.

In conclusion, we have studied the temperature and polarization dependence of magnetic fluctuations in nearly-optimal-doped NaFe_{0.9785}Co_{0.0215}As. While intensity of the resonance mode tracks the superconducting order parameter, energy of the mode only slightly softens approaching T_c . Anisotropic fluctuations in NaFe_{0.9785}Co_{0.0215}As are present for $E < 7$ meV and $T \lesssim 35$ K, and anisotropic fluctuations mostly become partially gapped inside the superconducting state, lacking the anisotropic resonance mode seen in BaFe₂As₂ superconductors near optimal doping. Nonetheless, behavior of anisotropic fluctuations in iron-based superconductors can be viewed to qualitatively reside somewhere along a continuous evolution, as exemplified by the evolution of anisotropic fluctuations in NaFe_{1-x}Co_xAs. However, the behavior of particular compounds appears to be material-specific, likely resulting from the interplay of superconducting gap energies and spin-orbit coupling.

V. ACKNOWLEDGMENTS

We thank Zhuang Xu and Huiqian Luo for assistance in resistivity change under uniaxial stress measurements. The single crystal growth and neutron scattering work at Rice is supported by the U.S. DOE, BES under Contract No. DE-SC0012311 (P.D.). The materials work at Rice is also supported by the Robert A. Welch Foundation Grant Nos. C-1839 (P.D.). This research used resources at the High Flux Isotope Reactor, a DOE Office of Science User Facility operated by the Oak Ridge National Laboratory.

* Electronic address: Yu.Song@rice.edu

† Electronic address: pdai@rice.edu

¹ D. J. Scalapino, Rev. Mod. Phys. **84**, 1383 (2012).

² P. C. Dai, Rev. Mod. Phys. **87**, 855 (2015).

³ D. S. Inosov, C. R. Phys. **17**, 60 (2016).

⁴ Jun Zhao, D. T. Adroja, Dao-Xin Yao, R. Bewley, Shiliang Li, X. F. Wang, G. Wu, X. H. Chen, Jiangping Hu, and Pengcheng Dai, Nat. Phys. **5**, 555-560 (2009).

⁵ L. W. Harriger, H. Q. Luo, M. S. Liu, C. Frost, J. P. Hu, M. R. Norman, and Pengcheng Dai, Phys. Rev. B **84**, 054544 (2011).

⁶ Chenglin Zhang, Leland W. Harriger, Zhiping Yin, Weicheng Lv, Miaoyin Wang, Guotai Tan, Yu Song, D. L. Abernathy, Wei Tian, Takeshi Egami, Kristjan Haule, Gabriel Kotliar, and Pengcheng Dai, Phys. Rev. Lett. **112**, 217202 (2014).

⁷ S. O. Diallo, V. P. Antropov, T. G. Perring, C. Broholm, J. J. Pulikkotil, N. Ni, S. L. Bud'ko, P. C. Canfield, A. Kreyssig, A. I. Goldman, and R. J. McQueeney, Phys. Rev. Lett. **102**, 187206 (2009).

⁸ R. A. Ewings, T. G. Perring, J. Gillett, S. D. Das, S. E.

Sebastian, A. E. Taylor, T. Guidi, and A. T. Boothroyd, Phys. Rev. B **83**, 214519 (2011).

⁹ Mengshu Liu, Leland W. Harriger, Huiqian Luo, Meng Wang, R. A. Ewings, T. Guidi, Hyowon Park, Kristjan Haule, Gabriel Kotliar, S. M. Hayden, and Pengcheng Dai, Nat. Phys. **8**, 376-381 (2012).

¹⁰ Ke-Jin Zhou, Yao-Bo Huang, Claude Monney, Xi Dai, Vladimir N. Strocov, Nan-Lin Wang, Zhi-Guo Chen, Chenglin Zhang, Pengcheng Dai, Luc Patthey, Jeroen van den Brink, Hong Ding, and Thorsten Schmitt, Nat. Commun. **4**, 1470 (2013).

¹¹ Meng Wang, Chenglin Zhang, Xingye Lu, Guotai Tan, Huiqian Luo, Yu Song, Miaoyin Wang, Xiaotian Zhang, E.A. Goremychkin, T.G. Perring, T.A. Maier, Zhiping Yin, Kristjan Haule, Gabriel Kotliar, and Pengcheng Dai, Nat. Commun. **4**, 2874 (2013).

¹² J. T. Park, D. S. Inosov, A. Yaresko, S. Graser, D. L. Sun, Ph. Bourges, Y. Sidis, Yuan Li, J.-H. Kim, D. Haug, A. Ivanov, K. Hradil, A. Schneidewind, P. Link, E. Faulhaber, I. Glavatsky, C. T. Lin, B. Keimer, and V. Hinkov, Phys. Rev. B **82**, 134503 (2010).

- ¹³ C. Zhang, M. Wang, H. Luo, M. Wang, M. Liu, J. Zhao, D. L. Abernathy, T. A. Maier, K. Marty, M. D. Lumsden, S. Chi, S. Chang, J. A. Rodriguez-Rivera, J. W. Lynn, T. Xiang, J. Hu, and P. Dai, *Sci. Rep.* **1**, 115 (2011).
- ¹⁴ Leland W. Harriger, Astrid Schneidewind, Shiliang Li, Jun Zhao, Zhengcai Li, Wei Lu, Xiaoli Dong, Fang Zhou, Zhongxian Zhao, Jiangping Hu, and Pengcheng Dai, *Phys. Rev. Lett.* **103**, 087005 (2009).
- ¹⁵ G. S. Tucker, R. M. Fernandes, D. K. Pratt, A. Thaler, N. Ni, K. Marty, A. D. Christianson, M. D. Lumsden, B. C. Sales, A. S. Sefat, S. L. Bud'ko, P. C. Canfield, A. Kreyssig, A. I. Goldman, and R. J. McQueeney, *Phys. Rev. B* **89**, 180503 (2014).
- ¹⁶ Stephen D. Wilson, Pengcheng Dai, Shiliang Li, Songxue Chi, H. J. Kang, and J. W. Lynn, *Nature* **442**, 59-52 (2006).
- ¹⁷ Miaoyin Wang, Huiqian Luo, Jun Zhao, Chenglin Zhang, Meng Wang, Karol Marty, Songxue Chi, Jeffrey W. Lynn, Astrid Schneidewind, Shiliang Li, and Pengcheng Dai, *Phys. Rev. B* **81**, 174524 (2010).
- ¹⁸ G. Yu, Y. Li, E. M. Motoyama, and M. Greven, *Nat. Phys.* **5**, 873 (2009).
- ¹⁹ D. S. Inosov, J. T. Park, A. Charnukha, Yuan Li, A. V. Boris, B. Keimer, and V. Hinkov, *Phys. Rev. B* **83**, 214520 (2011).
- ²⁰ Chenglin Zhang, Weicheng Lv, Guotai Tan, Yu Song, Scott V. Carr, Songxue Chi, M. Matsuda, A. D. Christianson, J. A. Fernandez-Baca, L. W. Harriger, and Pengcheng Dai, *Phys. Rev. B* **93**, 174522 (2016).
- ²¹ Qisi Wang, J. T. Park, Yu Feng, Yao Shen, Yiqing Hao, Bingying Pan, J. W. Lynn, A. Ivanov, Songxue Chi, M. Matsuda, Huibo Cao, R. J. Birgeneau, D. V. Efremov, and Jun Zhao, *Phys. Rev. Lett.* **116**, 197004 (2016).
- ²² C. H. Lee, K. Kihou, J. T. Park, K. Horigane, K. Fujita, F. Waßer, N. Qureshi, Y. Sidis, J. Akimitsu, and M. Braden, *Sci. Rep.* **6**, 23424 (2016).
- ²³ D. S. Inosov, J. T. Park, P. Bourges, D. L. Sun, Y. Sidis, A. Schneidewind, K. Hradil, D. Haug, C. T. Lin, B. Keimer, and V. Hinkov, *Nat. Phys.* **6**, 178-181 (2010).
- ²⁴ H. F. Fong, B. Keimer, D. Reznik, D. L. Milius, and I. A. Aksay, *Phys. Rev. B* **54**, 6708 (1996).
- ²⁵ C. Stock, C. Broholm, J. Hudis, H. J. Kang, and C. Petrovic, *Phys. Rev. Lett.* **100**, 087001 (2008).
- ²⁶ Leland W. Harriger, O. J. Lipscombe, Chenglin Zhang, Huiqian Luo, Meng Wang, Karol Marty, M. D. Lumsden, and Pengcheng Dai, *Phys. Rev. B* **85**, 054511 (2012).
- ²⁷ Chenglin Zhang, H.-F. Li, Yu Song, Yixi Su, Guotai Tan, Tucker Netherton, Caleb Redding, Scott V. Carr, Oleg Sobolev, Astrid Schneidewind, Enrico Faulhaber, L. W. Harriger, Shiliang Li, Xingye Lu, Dao-Xin Yao, Tanmoy Das, A. V. Balatsky, Th. Brückel, J. W. Lynn, and Pengcheng Dai, *Phys. Rev. B* **88**, 064504 (2013).
- ²⁸ P. D. Johnson, H.-B. Yang, J. D. Rameau, G. D. Gu, Z.-H. Pan, T. Valla, M. Weinert, and A. V. Fedorov, *Phys. Rev. Lett.* **114**, 167001 (2015).
- ²⁹ S. V. Borisenko, D. V. Evtushinsky, Z.-H. Liu, I. Morozov, R. Kappenberger, S. Wurmehl, B. Büchner, A. N. Yaresko, T. K. Kim, M. Hoesch, T. Wolf, and N. D. Zhigadlo, *Nat. Phys.* **12**, 311 (2016).
- ³⁰ A. Charnukha, K. W. Post, S. Thirupathiah, D. Pr opper, S. Wurmehl, M. Roslova, I. Morozov, B. B uchner, A. N. Yaresko, A. V. Boris, S. V. Borisenko, and D. N. Basov, *Sci. Rep.* **6**, 18620 (2016).
- ³¹ N. Qureshi, P. Steffens, S. Wurmehl, S. Aswartham, B. Büchner, and M. Braden, *Phys. Rev. B* **86**, 060410 (2012).
- ³² Chong Wang, Rui Zhang, Fa Wang, Huiqian Luo, L. P. Regnault, Pengcheng Dai, and Yuan Li, *Phys. Rev. X* **3**, 041036 (2013).
- ³³ Yu Song, Louis-Pierre Regnault, Chenglin Zhang, Guotai Tan, Scott V. Carr, Songxue Chi, A. D. Christianson, Tao Xiang, and Pengcheng Dai, *Phys. Rev. B* **88** 134512 (2013).
- ³⁴ Yu Song, Haoran Man, Rui Zhang, Xingye Lu, Chenglin Zhang, Meng Wang, Guotai Tan, L.-P. Regnault, Yixi Su, Jian Kang, Rafael M. Fernandes, and Pengcheng Dai, *Phys. Rev. B* **94**, 214516 (2016).
- ³⁵ Mingwei Ma, Philippe Bourges, Yvan Sidis, Yang Xu, Shiyang Li, Biaoyan Hu, Jiarui Li, Fa Wang, and Yuan Li, *Phys. Rev. X* **7**, 021025 (2017).
- ³⁶ P. Steffens, C. H. Lee, N. Qureshi, K. Kihou, A. Iyo, H. Eisaki, and M. Braden, *Phys. Rev. Lett.* **110**, 137001 (2013).
- ³⁷ Chenglin Zhang, Mengshu Liu, Yixi Su, Louis-Pierre Regnault, Meng Wang, Guotai Tan, Th. Brückel, Takeshi Egami, and Pengcheng Dai, *Phys. Rev. B* **87**, 081101 (2013).
- ³⁸ N. Qureshi, C. H. Lee, K. Kihou, K. Schmalzl, P. Steffens, and M. Braden, *Phys. Rev. B* **90**, 100502 (2014).
- ³⁹ Mengshu Liu, C. Lester, Jiri Kulda, Xinye Lu, Huiqian Luo, Meng Wang, S. M. Hayden, and Pengcheng Dai, *Phys. Rev. B*, **85**, 214516 (2012).
- ⁴⁰ Meng Wang, M. Yi, H. L. Sun, P. Valdivia, M. G. Kim, Z. J. Xu, T. Berlijn, A. D. Christianson, Songxue Chi, M. Hashimoto, D. H. Lu, X. D. Li, E. Bourret-Courchesne, Pengcheng Dai, D. H. Lee, T. A. Maier, and R. J. Birgeneau, *Phys. Rev. B* **93**, 205149 (2016).
- ⁴¹ Chenglin Zhang, Rong Yu, Yixi Su, Yu Song, Miaoyin Wang, Guotai Tan, Takeshi Egami, J. A. Fernandez-Baca, Enrico Faulhaber, Qimiao Si, and Pengcheng Dai, *Phys. Rev. Lett.* **111**, 207002 (2013).
- ⁴² Chenglin Zhang, Yu Song, L.-P. Regnault, Yixi Su, M. Enderle, J. Kulda, Guotai Tan, Zachary C. Sims, Takeshi Egami, Qimiao Si, and Pengcheng Dai, *Phys. Rev. B* **90**, 140502 (2014).
- ⁴³ Guotai Tan, Yu Song, Chenglin Zhang, Lifang Lin, Zhuang Xu, Tingting Hou, Wei Tian, Huibo Cao, Shiliang Li, Shiping Feng, and Pengcheng Dai, *Phys. Rev. B* **94**, 014509 (2016).
- ⁴⁴ Ding Hu *et al.*, unpublished polarized neutron scattering results on BaFe₂As_{1.4}P_{0.6}.
- ⁴⁵ N. S. Headings, S. M. Hayden, J. Kulda, N. H. Babu, and D. A. Cardwell, *Phys. Rev. B* **84**, 104513 (2011).
- ⁴⁶ N. Spyrison, M. A. Tanatar, Kyuil Cho, Y. Song, P. C. Dai, C. L. Zhang, and R. Prozorov, *Phys. Rev. B* **86**, 144528 (2012).
- ⁴⁷ Scott V. Carr, Chenglin Zhang, Yu Song, Guotai Tan, Yu Li, D. L. Abernathy, M. B. Stone, G. E. Granroth, T. G. Perring, and Pengcheng Dai, *Phys. Rev. B* **93**, 214506 (2016).
- ⁴⁸ S. L. Li, C. de la Cruz, Q. Huang, G. F. Chen, T.-L. Xia, J. L. Luo, N. L. Wang, and P. C. Dai, *Phys. Rev. B* **80**, 020504 (2009).
- ⁴⁹ K. Terashima, Y. Sekiba, J. H. Bowen, K. Nakayama, T. Kawahara, T. Sato, P. Richard, Y.-M. Xu, L. J. Li, G. H. Cao, Z.-A. Xu, H. Ding, and T. Takahashi, *Proc. Natl. Acad. Sci. U.S.A.* **106**, 7330-7333 (2009).
- ⁵⁰ Yu Song, John Van Dyke, I. K. Lum, B. D. White, Sooyoung Jang, Duygu Yazici, L. Shu, A. Schneidewind, Petr Čermák, Y. Qiu, M. B. Maple, Dirk K. Morr, and

- Pengcheng Dai, Nat. Commun. **7**, 12774 (2016).
- ⁵¹ M. G. Kim, G. S. Tucker, D. K. Pratt, S. Ran, A. Thaler, A. D. Christianson, K. Marty, S. Calder, A. Podlesnyak, S. L. Bud'ko, P. C. Canfield, A. Kreyssig, A. I. Goldman, and R. J. McQueeney, Phys. Rev. Lett. **110**, 177002 (2013).
- ⁵² Huiqian Luo, Meng Wang, Chenglin Zhang, Xingye Lu, Louis-Pierre Regnault, Rui Zhang, Shiliang Li, Jiangping Hu, and Pengcheng Dai, Phys. Rev. Lett. **111**, 107006 (2013).
- ⁵³ Hsueh-Hui Kuo, Jiun-Haw Chu, Johanna C. Palmstrom, Steven A. Kivelson, Ian R. Fisher, Science **352**, 958 (2016).
- ⁵⁴ Zhaoyu Liu, Yanhong Gu, Wei Zhang, Dongliang Gong, Wenliang Zhang, Tao Xie, Xingye Lu, Xiaoyan Ma, Xiaotian Zhang, Rui Zhang, Jun Zhu, Cong Ren, Lei Shan, Xi-anggang Qiu, Pengcheng Dai, Yi-feng Yang, Huiqian Luo, and Shiliang Li, Phys. Rev. Lett. **117**, 157002 (2016).
- ⁵⁵ Yanhong Gu, Zhaoyu Liu, Tao Xie, Wenliang Zhang, Dongliang Gong, Ding Hu, Xiaoyan Ma, Chunhong Li, Lingxiao Zhao, Lifang Lin, Zhuang Xu, Guotai Tan, Genfu Chen, Zi Yang Meng, Yi-feng Yang, Huiqian Luo, and Shiliang Li, Phys. Rev. Lett. **119**, 157001 (2017).
- ⁵⁶ F. Waßer, C. H. Lee, K. Kihou, P. Steffens, K. Schmalzl, N. Qureshi, and M. Braden, Sci. Rep. **7**, 10307 (2017).
- ⁵⁷ Yu Li, Weiyi Wang, Yu Song, Haoran Man, Xingye Lu, Frédéric Bourdarot, and Pengcheng Dai, Phys. Rev. B **96**, 020404 (2017).
- ⁵⁸ Jiun-Haw Chu, Hsueh-Hui Kuo, James G. Analytis, and Ian R. Fisher, Science **337**, 710-712 (2012).
- ⁵⁹ Guotai Tan, Ping Zheng, Xiancheng Wang, Yanchao Chen, Xiaotian Zhang, Jianlin Luo, Tucker Netherton, Yu Song, Pengcheng Dai, Chenglin Zhang, and Shiliang Li, Phys. Rev. B **87**, 144512 (2013).